Pattern Transition in Spacecraft Formation Flying using Bifurcating Potential Fields

Derek J. Bennet, Colin R. McInnes

Department of Mechanical Engineering, University of Strathclyde, Glasgow, G1 1XJ, Scotland, United Kingdom

Abstract

Many new and exciting space mission concepts have developed around spacecraft formation flying, allowing for autonomous distributed systems that can be robust, scalable and flexible. This paper considers the development of a new methodology for the control of multiple spacecraft. Based on the artificial potential function method, research in this area is extended by considering the new approach of using bifurcation theory as a means of controlling the transition between different formations. For real, safety or mission critical applications it is important to ensure that desired behaviours will occur. Through dynamical systems theory, this paper also aims to provide a step in replacing traditional algorithm validation with mathematical proof, supported through simulation. This is achieved by determining the non-linear stability properties of the system, thus proving the existence or not of desired behaviours. Practical considerations such as the issue of actuator saturation and communication limitations are addressed, with the development of a new bounded control law based on bifurcating potential fields providing the key contribution of this paper. To illustrate spacecraft formation flying using the new methodology formation patterns are considered in low-Earth-orbit utilising the Clohessy-Wiltshire relative linearised equations of motion. It is shown that a formation of spacecraft can be driven safely onto equally spaced projected circular orbits, autonomously reconfiguring between them, whilst satisfying constraints made regarding each spacecraft.

Keywords: Spacecraft formation flying, bifurcating potential fields

1. Introduction

Spacecraft formation flying (SFF) has emerged as an important type of distributed spacecraft system that enables a variety of missions that can improve significantly the functionality of the system in comparison with a large single spacecraft [26]. SFF is defined by Gill et al. [10] "*as a technology, that includes two or more spacecraft in a tightly controlled spatial configuration, whose operations are closely synchronised*". Many new and exciting space mission have been developed around this technology such as interferometric/sparse aperture missions. The Stellar Imager is an example of such a mission that consists of a UV/Optical deep-space telescope composed of approximately 30 one-meter array elements [6]. Another example is the DARWIN mission that will consist of 6 spacecraft equipped with optical telescopes in formation at the Sun-Earth L_2 point [35].

There have been several control architectures proposed for SFF, with Scharf et al. [28] and Lawton [17] defining five of the most popular control architectures as; Multiple-Input, Multiple-Output (MIMO), Virtual Structure (VS), Leader/Follower (L/F), cyclic and behavioral.

MIMO follows the multiple-input, multiple-output methodology, considering the relative states of the formations as a single plant [29]. The advantage of this system is that optimality can be guaranteed, however, the controller can become unstable with the failure of one spacecraft [28]. The VS system is a centralised control architecture where all spacecraft in the formation are part of a virtual rigid structure where changes in the position of each spacecraft are communicated with a formation controller and the appropriate alterations are made to the structure [14]. The system has the advantage of maintaining a formation well during manoeuvrers [25], however, it does not perform well if the formation shape is time-varying and is also susceptible to failure as it is centralised control [7].

The L/F architecture is a centralised hierarchical control scheme where one spacecraft obtains information on a desired trajectory and follower spacecraft track the leader [36, 38]. The Landsat-7 and Earth Observing-1 (EO-1) satellites are examples of a real hierarchical L/F mission and is generally considered the first mission to demonstrate formation flying [26]. The two satellites in this formation do not communicate with each other directly.

Instead a central controller determines Landsat-7's position and sends this information to EO-1 determining the future orbits of both spacecraft [3]. The limitation of this system is that it is also dependent upon the central controller and is therefore susceptible to failure. In addition as the number of spacecraft increase, the workload required to maintain a formation discretely will increase significantly. Cyclic controller architectures are similar to the L/F however each spacecraft are connected in a non-hierarchical way [12].

A promising approach to overcome the limitations of the architectures discussed is to develop behavioral control architectures in which all spacecraft interact producing an emergent global behaviour. An example of a behavioural control architecture is the artificial potential field method [20] that is used throughout this paper. This distributed approach can allow for spacecraft to be driven autonomously to desired goal positions, whilst ensuring collision avoidance, and can be considered flexible and robust to individual spacecraft failures. It has been used successfully, for example, by Reif and Wang as a form of distributed behavioral control for autonomous robots [24], by Badawy and McInnes in autonomous structure assembly [1] and by Izzo [13] and McQuade [21] for SFF.

For real, safety or mission critical applications it is essential that the behaviour of the spacecraft be verified to ensure that no unwanted behaviours will occur. Through the use of dynamical systems theory this paper aims to take steps towards replacing algorithm validation with mathematical proof, supported by simulation. In addition Winfield [37] has introduced the term *swarm engineering* to highlight the key issues that are involved in real, safety or mission critical applications as opposed to those based only on simulation. To this end this paper addresses issues of actuator saturation and communication limitations. The key contribution that this paper presents is in the development of a new SFF bounded control law based on bifurcating potential fields. To illustrate SFF using the new methodology, formation patterns are considered in low-Earth-orbit utilising the Clohessy-Wiltshire relative linearised equations of motion. It is shown that a formation of spacecraft can be driven safely onto equally spaced projected circular orbits, autonomously reconfiguring between them, whilst satisfying constraints made regarding actuator limit and communication range of each spacecraft. Although the method is not fuel optimal it is seen as an effective means of controlling complex reformation manoeuvres only, with station-keeping be-

tween the manoeuvres using classical optimal control methods.

The paper proceeds as follows. In the next section the basic SFF model is described, explaining the artificial potential field method and bifurcation theory. The linear and non-linear stability of the model is also discussed. Section 3 shows the results of numerical simulations carried out, whilst Section 4 considers the real problem of actuator saturation and communication constraints, develops a set of new bounded control laws and applies them to achieve SFF in low-Earth-orbit satisfying assumptions made regarding each spacecraft.

2. Formation Model

2.1. Model and Basic Formation Properties

Consider a swarm of homogeneous autonomous spacecraft ($1 \leq i \leq N$) interacting via an artificial potential function, U. It will be initially assumed that all spacecraft are operating in free-space, are fully actuated and can communicate with each other. The gradient of the artificial potential defines a virtual force acting on each spacecraft so that the dynamics of each spacecraft in an inertial frame of reference can be expressed as

$$\frac{d\mathbf{x}_i}{dt} = \mathbf{v}_i \tag{1}$$

$$m\frac{d\mathbf{v}_i}{dt} = -\nabla_i U^S(\mathbf{x}_i) - \nabla_i U^R(\mathbf{x}_{ij}) - \sigma\mathbf{v}_i \tag{2}$$

where m is the mass of each spacecraft, ($\mathbf{x}_i$, $\mathbf{v}_i$) are the position and velocity of each spacecraft respectively and $\sigma > 0$ controls the amplitude of the dissipation control term.

From Eq. 2 it can be seen that the virtual force experienced by each spacecraft is dependent upon the gradient of two different artificial potential functions and a dissipative term. The first term in Eq. 2 is defined as the *Steering Potential*, U^S, which will control the formation and force each spacecraft to a desired position, whereas the second term in Eq. 2 is defined as the *Repulsive Potential*, U^R, which ensures collision avoidance and an equally spaced final formation.

The *Repulsive Potential*, based on a generalized pairwise Morse potential [8], is

$$U_{ij}^{R} = \sum_{j,j\neq i} C_r \exp^{-|\mathbf{x}_{ij}|/L_r} \tag{3}$$

where C_r and L_r represent the amplitude and length-scale of *Repulsive Potential* respectively and $|\mathbf{x}_{ij}| = |\mathbf{x}_i - \mathbf{x}_j|$.

The total repulsive force on the i^{th} spacecraft is dependent upon the position of all the other $(N-1)$ spacecraft in the formation. The *Repulsive Potential* is therefore used to ensure that as the spacecraft are steered towards the goal state they do not collide with each other. Once all the spacecraft have been driven to the desired equilibrium state the *Repulsive Potential* also ensures that they are equally spaced for symmetric formations.

Before considering the model further, it is useful to establish some basic properties of a system of spacecraft interacting via an internal pair-wise potential function and a dissipative term as follows

$$m\dot{\mathbf{v}}_i = -\nabla_i U(\mathbf{x}_{ij}) - \sigma \mathbf{v}_i \tag{4}$$

Taking the dot product of the velocity vector with Eq. 4 and summing over all the spacecraft results in

$$\sum_i m\mathbf{v}_i \cdot \dot{\mathbf{v}}_i = -\sum_i \nabla_i U(\mathbf{x}_{ij}) \cdot \mathbf{v}_i - \sum_i \sigma \mathbf{v}_i \cdot \mathbf{v}_i \tag{5}$$

Thus, the rate of change of total effective energy, E, of the system is continually decreasing, as shown in Eq. 6, until the system reaches an equilibrium state

$$\frac{dE}{dt} = -\sigma \sum_i |\mathbf{v}_i|^2 \leq 0 \tag{6}$$

where $E = \frac{1}{2}\left[\sum_i m|\mathbf{v}_i|^2 + \sum_i U(\mathbf{x}_{ij})\right]$.

Also, taking the cross product of the position vector with Eq. 4 and summing over all the spacecraft results in

$$\sum_i m\mathbf{x}_i \times \dot{\mathbf{v}}_i = -\sum_i \mathbf{x}_i \times \nabla_i U(\mathbf{x}_{ij}) - \sum_i \sigma \mathbf{x}_i \times \mathbf{v}_i \tag{7}$$

Defining the angular momentum, $\mathbf{H} = \sum_i \mathbf{x}_i \times \mathbf{v}_i$ it can be shown that the rate of change of angular momentum will also be continually decreasing until the system reaches an equilibrium defined by

$$\left|\frac{d\mathbf{H}}{dt}\right| = -\left(\frac{\sigma}{m}\right)|\mathbf{H}| \leq 0 \tag{8}$$

since $\sum_i \mathbf{x}_i \times \nabla_i U(\mathbf{x}_{ij}) = 0$ due to internal symmetry in the formation [19].

Finally, consider the position, velocity and acceleration vector of the center-of-mass as follows

$$\mathbf{R}_c = \frac{\sum_i m\mathbf{x}_i}{\sum_i m}, \quad \dot{\mathbf{R}}_c = \frac{\sum_i m\mathbf{v}_i}{\sum_i m}, \quad \ddot{\mathbf{R}}_c = \frac{\sum_i m\dot{\mathbf{v}}_i}{\sum_i m} \tag{9}$$

Summing over all the spacecraft it can then be shown that the system of spacecraft can be treated as if it were a single spacecraft, so that the equations of motion for the swarm center-of-mass are

$$m\ddot{\mathbf{R}}_c = -\sigma\dot{\mathbf{R}}_c \tag{10}$$

where $\sum_i \nabla_i U(\mathbf{x}_{ij}) = 0$ due to internal symmetry in the formation.

Therefore, the model and some useful properties of a formation of spacecraft have been discussed that will become useful in the following sections.

2.2. Artificial Potential Function Scale Separation

As noted in the previous section the force experienced by each spacecraft is dependent upon the gradient of two different artificial potential functions. The *Steering Potential* is a function of position only, with length scale R, whereas the *Repulsive Potential*, noted in the previous section, has length scale L_r as follows

$$U^S = f(X, R) \tag{11}$$

$$U^R = C_r \exp^{-X/L_r} \tag{12}$$

For illustration consider a simple 1-dimensional system with position coordinate X.

Defining an outer region dependent upon the *Steering Potential* only and an inner region dependent upon the *Repulsive Potential* only it can be shown that these two regions are separated so that each *agent* moves under the influence of the long-range *Steering Potential* but with short-range collision avoidance (for $L_r/R << 1$). This effectively creates a boundary layer between them, as illustrated in Fig. 1, where the position of the boundary layer is dependent upon the parameters chosen in the *Steering* and *Repulsive Potentials*. This can then be used to determine the non-linear stability properties of the system considering the *Steering Potential* only.

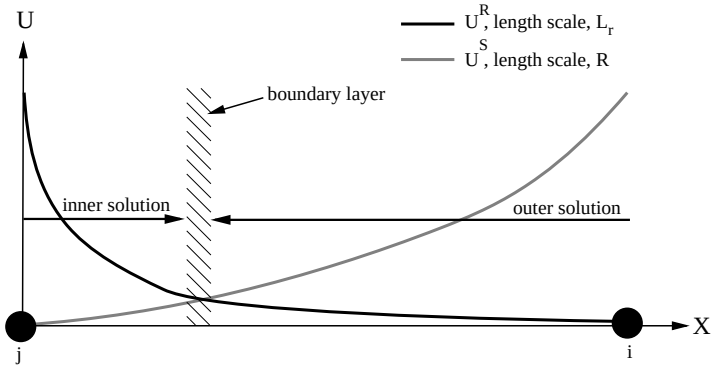

Figure 1: Artificial potential function scale separation

For 1D motion of a spacecraft, of mass m and damping constant σ, the equations of motion are

$$m\frac{dV}{dt} = -\frac{dU^R}{dX} - \frac{dU^S}{dX} - \sigma V \tag{13}$$

so that

$$mV\frac{dV}{dX} = \frac{C_r}{L_r}\exp^{-X/L_r} - \frac{dU^S}{dX} - \sigma V \tag{14}$$

Scaling X such that $S = X/R$, then

$$\frac{1}{R}mV\frac{dV}{dS} = \frac{C_r}{L_r}\exp^{-\frac{R}{L_r}S} - \frac{1}{R}\frac{dU^S}{dS} - \sigma V \tag{15}$$

Now define $\varepsilon = \dfrac{L_r}{R} << 1$ so that

$$mV\frac{dV}{dS} = \frac{C_r}{\varepsilon}\exp^{-\frac{S}{\varepsilon}} - \frac{dU^S}{dS} - \sigma RV \tag{16}$$

Let $\varepsilon \to 0$ in order to consider far-field dynamics which form a singularly perturbed system [4]

$$\lim_{\varepsilon \to 0} \frac{1}{\varepsilon}\exp^{(-S/\varepsilon)} = 0 \tag{17}$$

Therefore, at large separation distances the *Repulsive Potential* vanishes allowing the consideration of the *Steering Potential* only when investigating the stability of the system, under the assumption that $\epsilon << 1$.

Conversely defining a stretched variable $\overline{S} = \dfrac{S}{\varepsilon}$ it is found that the near-field dynamics are defined by

$$mV\frac{dV}{d\overline{S}} = C_r\exp^{-\overline{S}} - \varepsilon R\left(\frac{1}{L_r}\frac{dU^S}{d\overline{S}} + \sigma V\right) \tag{18}$$

and letting $\varepsilon \to 0$

$$mV\frac{dV}{d\overline{S}} = C_r\exp^{-\overline{S}} \tag{19}$$

Thus, at small separations the *Steering Potential* vanishes. Therefore, it has be shown that a scale separation exists in the model between the *Steering* and *Repulsive* terms allowing for the treatment of collisions as separate in the subsequent stability analysis.

2.3. 1-Parameter Static Bifurcation

Referring back to Eq. 2 the *Steering Potential* is based on the new approach of bifurcating potential fields. As an example consider the use of the *pitchfork bifurcation* [15], as shown in the first two terms of Eq. 20. The aim of this potential is to drive each spacecraft to a goal distance, r, from the

origin in the x-y plane thus forming a symmetric ring. The last term in Eq. 20 is to ensure that the formation is created in the x-y plane.

$$U^S(\mathbf{x}_i;\mu,\alpha) \;=\; -\frac{1}{2}\mu\left(\rho_i - r\right)^2 + \frac{1}{4}\left(\rho_i - r\right)^4 + \frac{1}{2}\alpha z_i^2 \tag{20}$$

where cylindrical polar coordinates (ρ_i, z_i) are now used, neglecting the θ term as the potential field is rotationally symmetric, μ is the bifurcation parameter, r is a constant and α controls the amplitude of the quadratic potential.

Depending on the sign of μ, the *Steering Potential* can have two distinct forms. Figure 2 shows how the potential bifurcates from a single minimum into two minimum when $\mu = 0$, while Fig. 3 shows the shape of the potential when $\mu < 0$ and $\mu > 0$ $(r = 5)$.

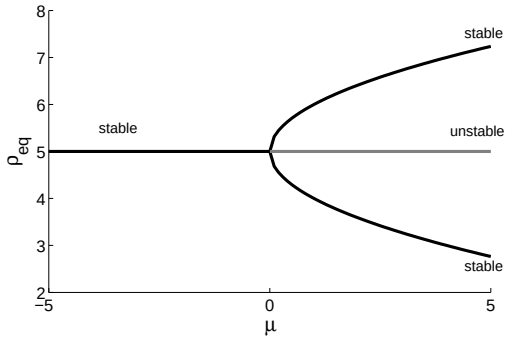

Figure 2: Pitchfork bifurcation diagram

The equilibrium states of the potential occurs whenever $\partial U/\partial\rho_i = 0$ and $\partial U/\partial z_i = 0$. Therefore,

$$\frac{\partial U}{\partial \rho_i} = -\mu(\rho_i - r) + (\rho_i - r)^3 \tag{21}$$

$$\frac{\partial U}{\partial z_i} = \alpha z_i \tag{22}$$

If $\mu \leq 0$ equilibrium occurs when $\rho_i = r$. If $\mu > 0$ equilibrium occurs when $\rho_i = r$, $r \pm \sqrt{\mu}$. Therefore, a single ring will bifurcate to a double ring

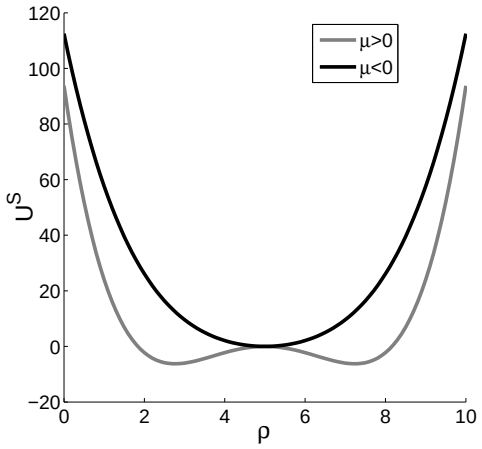

Figure 3: Pitchfork potential

using μ as a control parameter.

For a function consisting of two variables the stability of the system is determined from the sign of the determinant of the Hessian matrix[23], D, is

$$D = \frac{\partial^2 U}{\partial \rho_i^2}\frac{\partial^2 U}{\partial z_i^2} - \left[\frac{\partial^2 U}{\partial \rho_i \partial z_i}\right]^2 \tag{23}$$

The conditions for stability are
(i) $D > 0$, $\partial^2 U/\partial \rho_i^2 > 0 \Longrightarrow$ equilibrium point is a stable minimum.
(ii) $D > 0$, $\partial^2 U/\partial \rho_i^2 < 0 \Longrightarrow$ equilibrium point is a unstable maximum.
(iii) $D < 0 \Longrightarrow$ equilibrium point is a saddle.

The second derivative of the potential is as follows

$$\frac{\partial^2 U}{\partial \rho_i^2} = -\mu + 3(\rho_i - r)^2 \tag{24}$$

$$\frac{\partial^2 U}{\partial z_i^2} = \alpha \tag{25}$$

$$\frac{\partial^2 U}{\partial \rho_i \partial z_i} = 0 \tag{26}$$

From Eq. 25 as α is positive, $\partial^2 U/\partial z_i^2 > 0$. From Eq. 24 it can be seen that $\partial^2 U/\partial \rho_i^2 \gtrless 0$ depending on the values of μ. Therefore, the properties of the equilibrium state ρ_{eq} are shown in table 1

Table 1: Stability of equilibrium states of artificial potential function

Bifurcation parameter, μ	Equilibrium position, ρ_{eq}	$\partial^2 U/\partial \rho_i^2$	Stability
< 0	r	> 0	stable minimum
> 0	r	< 0	unstable maximum
	$r + \sqrt{\mu}$	> 0	stable minimum
	$r - \sqrt{\mu}$	> 0	stable minimum

2.3.1. Linear stability: 1*-parameter static bifurcation*

To determine the linear stability of a system of spacecraft subject to such a 1-parameter bifurcation *Steering Potential* an eigenvalue analysis is performed on the linearised equations of motion assuming that at large separation distances the *Repulsive Potential* can be neglected through scale separation as explained in Section 2.2. The linear stability analysis will be used to determine the local behaviour of the system by calculating its eigenvalue spectrum. Therefore, the equations of motion for the model are re-cast as

$$\begin{aligned} \begin{pmatrix} \dot{\mathbf{x}}_i \\ \dot{\mathbf{v}}_i \end{pmatrix} &= \begin{pmatrix} \mathbf{v}_i \\ -\sigma \mathbf{v}_i - \nabla_i U^S(\mathbf{x}_i) \end{pmatrix} \\ &= \begin{pmatrix} f(\mathbf{x}_i, \mathbf{v}_i) \\ g(\mathbf{x}_i, \mathbf{v}_i) \end{pmatrix} \end{aligned} \tag{27}$$

Let $\mathbf{x}_o$ and $\mathbf{v}_o$ denote fixed points with $\dot{\mathbf{x}}_i = \dot{\mathbf{v}}_i = 0$ so that

$$f(\mathbf{x}_o, \mathbf{v}_o) = 0 \tag{28}$$

$$g(\mathbf{x}_o, \mathbf{v}_o) = 0 \tag{29}$$

Thus, $\mathbf{v}_o = 0$ and $\nabla U^S = 0$ at equilibrium. This occurs when $\rho_o = r$ if $\mu < 0$ and $\rho_o = r, r \pm \sqrt{\mu}$ if $\mu > 0$, with $z_o = 0$. Defining $\delta \mathbf{x}_i = \mathbf{x}_i - \mathbf{x}_o$ and $\delta \mathbf{v}_i = \mathbf{v}_i - \mathbf{v}_o$ and Taylor Series expanding about the fixed points to linear order the eigenvalues of system can be found using

$$\begin{pmatrix} \delta\dot{\mathbf{x}}_i \\ \delta\dot{\mathbf{v}}_i \end{pmatrix} = \mathbf{J} \begin{pmatrix} \delta\mathbf{x}_i \\ \delta\mathbf{v}_i \end{pmatrix} \tag{30}$$

where,

$$\mathbf{J} = \left(\begin{array}{cc} \frac{\partial}{\partial \mathbf{x}_i}(f(\mathbf{x}_i, \mathbf{v}_i)) & \frac{\partial}{\partial \mathbf{v}_i}(f(\mathbf{x}_i, \mathbf{v}_i)) \\ \frac{\partial}{\partial \mathbf{x}_i}(g(\mathbf{x}_i, \mathbf{v}_i)) & \frac{\partial}{\partial \mathbf{v}_i}(g(\mathbf{x}_i, \mathbf{v}_i)) \end{array} \right)\Bigg|_{\mathbf{x}_o, \mathbf{v}_o} \tag{31}$$

The Jacobian, $\mathbf{J}$, is then a 4×4 matrix given by

$$\mathbf{J} = \left(\begin{array}{cccc} 0 & 0 & 1 & 0 \\ 0 & 0 & 0 & 1 \\ -\frac{\partial^2 U}{\partial \rho_i^2} & -\frac{\partial^2 U}{\partial \rho_i \partial z_i} & -\sigma & 0 \\ -\frac{\partial^2 U}{\partial \rho_i \partial z_i} & -\frac{\partial^2 U}{\partial z_i^2} & 0 & -\sigma \end{array} \right)\Bigg|_{\mathbf{x}_o, \mathbf{v}_o} \tag{32}$$

Substituting a trial exponential solution into Eq. 30, the eigenvalues, λ, of the system are found when $det(\mathbf{J} - \lambda\mathbf{I}) = 0$.

As shown previously, if $\mu < 0$ equilibrium of the system occurs when $\mathbf{x}_o = (r, 0)$ and $\mathbf{v}_i = 0$. Evaluating the Jacobian matrix given in Eq. 32 it is found that

$$\mathbf{J} = \begin{pmatrix} 0 & 0 & 1 & 0 \\ 0 & 0 & 0 & 1 \\ \mu & 0 & -\sigma & 0 \\ 0 & -\alpha & 0 & -\sigma \end{pmatrix} \tag{33}$$

The corresponding eigenvalue spectrum is therefore,

$$\lambda = \begin{cases} 1/2(-\sigma \pm \sqrt{(\sigma^2 - 4\alpha)}) \\ 1/2(-\sigma \pm \sqrt{(\sigma^2 + 4\mu)}) \end{cases} \tag{34}$$

As $\alpha > 0$, $\sigma > 0$ and $\mu < 0$ the eigenvalues are always either negative real or complex with negative real part as $-\sigma \pm \sqrt{(\sigma^2 - 4\alpha)} \not> 0$ and $-\sigma \pm \sqrt{(\sigma^2 + 4\mu)} \not> 0$. The equilibrium position can therefore be considered as linearly stable.

If $\mu > 0$ equilibrium of the system occurs when $\mathbf{x}_{o1} = (r, 0)$, $\mathbf{x}_{o2} = (r + \sqrt{\mu}, 0)$ and $\mathbf{x}_{o3} = (r - \sqrt{\mu}, 0)$ with $\mathbf{v}_i = 0$. The Jacobian matrix evaluated

at the three different equilibrium positions is given by Eq. 35, 36 and 37 respectively as

$$\mathbf{J}_1 = \begin{pmatrix} 0 & 0 & 1 & 0 \\ 0 & 0 & 0 & 1 \\ \mu & 0 & -\sigma & 0 \\ 0 & -\alpha & 0 & -\sigma \end{pmatrix} \tag{35}$$

$$\mathbf{J}_2 = \begin{pmatrix} 0 & 0 & 1 & 0 \\ 0 & 0 & 0 & 1 \\ -2\mu & 0 & -\sigma & 0 \\ 0 & -\alpha & 0 & -\sigma \end{pmatrix} \tag{36}$$

$$\mathbf{J}_3 = \begin{pmatrix} 0 & 0 & 1 & 0 \\ 0 & 0 & 0 & 1 \\ -2\mu & 0 & -\sigma & 0 \\ 0 & -\alpha & 0 & -\sigma \end{pmatrix} \tag{37}$$

The eigenvalues for $\mathbf{J}_1$ are

$$\lambda = \begin{cases} 1/2\left(-\sigma \pm \sqrt{(\sigma^2 - 4\alpha)}\right) \\ 1/2\left(-\sigma \pm \sqrt{(\sigma^2 + 4\mu)}\right) \end{cases} \tag{38}$$

Considering the second pair of eigenvalues in Eq. 38 it can be shown that $-\sigma \pm \sqrt{(\sigma^2 + 4\mu)} > 0$ since, $\sigma^2 + 4\mu > \sigma^2$ and therefore there will always be at least one positive real eigenvalue. This equilibrium position is therefore always linearly unstable.

The eigenvalues for $\mathbf{J}_2$ and $\mathbf{J}_3$ are

$$\lambda = \begin{cases} 1/2\left(-\sigma \pm \sqrt{(\sigma^2 - 4\alpha)}\right) \\ 1/2\left(-\sigma \pm \sqrt{(\sigma^2 - 8\mu)}\right) \end{cases} \tag{39}$$

Again as $\alpha > 0$, $\sigma > 0$ and $\mu > 0$ the eigenvalues are always either negative real or complex with negative real part as $-\sigma \pm \sqrt{(\sigma^2 - 4\alpha)} \not> 0$ and $-\sigma \pm \sqrt{(\sigma^2 - 8\mu)} \not> 0$. The equilibrium positions can therefore be considered as linearly stable.

2.3.2. Non-linear stability: 1-parameter static bifurcation

Using Lyapunov's second method the non-linear stability of the system can be investigated allowing an analytical proof that the swarm will relax into the minimum energy configuration. Again using the assumption of scale separation, the Lyapunov function, L, is defined as the total energy of the system, so that for unit mass

$$L = \sum_i \left(\frac{1}{2} |\mathbf{v}_i|^2 + U^S(\mathbf{x}_i) \right) \tag{40}$$

where $L > 0$ other than at the goal state when $L = 0$.

The rate of change of the Lyapunov function can be expressed as

$$\frac{dL}{dt} = \left(\frac{\partial L}{\partial \mathbf{x}_i} \right) \dot{\mathbf{x}}_i + \left(\frac{\partial L}{\partial \mathbf{v}_i} \right) \dot{\mathbf{v}}_i \tag{41}$$

Then, substituting Eq. 27 into Eq. 41 it can be seen that

$$\frac{dL}{dt} = -\sigma \sum_i |\mathbf{v}_i|^2 \leq 0 \tag{42}$$

A problem arises in the use of superimposed artificial potential functions as $\dot{L} \leq 0$. This implies that $\dot{L}$ could equal zero in a position other than the goal minimum suggesting that the system may become trapped in a local minimum. To ensure that the system is asymptotically stable to the desired goal state, the LaSalle Invariance principle can be used [16]. It extends the above constraints to state that if $L(0) = \dot{L}(0) = 0$ and the set $\{\mathbf{x}_i | \dot{L} = 0\}$ only occurs when $\mathbf{x}_i = \mathbf{x}_o$, then the goal state is asymptotically stable. Therefore, under the assumption of scale separation as there is a smooth, well defined symmetric potential field and equilibrium only occurs at the goal states, the local minima problem can be avoided and the system will relax into the desired goal position.

For the more general case when scale separation cannot be assumed, a similar analysis to that shown in **Section 2.1** can be used. Therefore, taking the dot product of the velocity vector with Eq. 2 and summing over all spacecraft results in

$$\sum_i m\mathbf{v}_i \cdot \dot{\mathbf{v}}_i = -\sum_i \sigma \mathbf{v}_i \cdot \mathbf{v}_i - \sum_i \nabla_i U^S(\mathbf{x}_i) \cdot \mathbf{v}_i - \sum_i \nabla_i U^R(\mathbf{x}_{ij}) \cdot \mathbf{v}_i \quad (43)$$

Thus, the rate of change of the total effective energy is then

$$\frac{dE}{dt} = -\sigma \sum_i |\mathbf{v}_i|^2 \leq 0 \quad (44)$$

where $E = \frac{1}{2}\sum_i m\mathbf{v}_i^2 + \sum_i U^S(\mathbf{x}_i) + \frac{1}{2}\sum_i U^R(\mathbf{x}_{ij})$.

This is a similar result to that obtained above, however, it now takes into consideration the *Repulsive Potential* field. Again, the total effective energy of the system is continually decreasing. However, the system may relax into a minimum energy configuration other than that given by the minimum of the desired *Steering Potential*. For example, considering the case when $r = 0$, each spacecraft will be driven to the origin of the system. However, due to the interaction with the *Repulsive Potential*, the spacecraft will be forced apart with the *Steering* and *Repulsive Potential* balancing such that the system will relax into a locally minimum energy cluster configuration. In this situation the scale separation argument does not hold true, however, it does provide a tool to enable analytical investigation of the stability of the problem.

3. Numerical Results

Figure 4 shows the evolution of a swarm of 40 spacecraft using the pitchfork bifurcating potential field as a means of the controlling the formation such that through a simple parameter change the swarm will autonomously form a double ring pattern and then bifurcate into a cluster and then a single ring formation. Each point-mass spacecraft, assumed to be operating in free-space, are given random initial conditions for position and velocity, with $C_r = 1$, $L_r = 0.5$, $\alpha = 2$ and $\sigma = 2$.

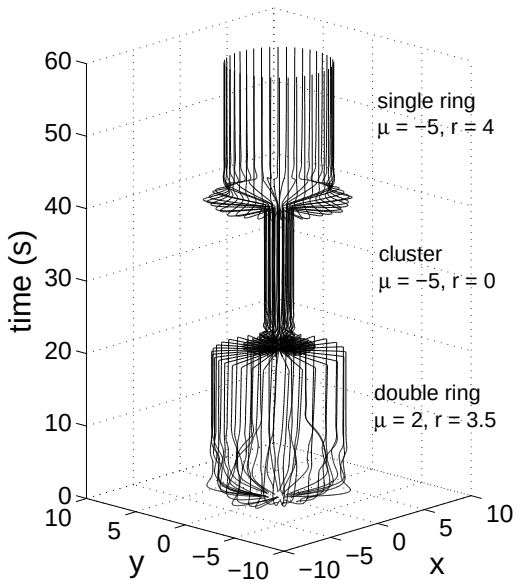

Figure 4: Evolution of swarm in the $x - y$ plane

Figures 5 (i)-(vi) show the results for the pitchfork bifurcating system indicating that the desired swarm patterns were achieved. The first pattern corresponds to the case when there are two stable equilibrium positions with $\mu > 0$, resulting in the spacecraft falling into a double ring pattern, as shown in Fig. 5 (ii). The bifurcation parameter is then altered such that $\mu < 0$ and $r = 0$ thus forcing each spacecraft to the origin with the repulsive potential causing an equally spaced cluster to form, as shown in Fig. 5 (iv). The swarm then bifurcates once more so that $r = 5$ and an equally spaced ring pattern emerges, as shown in Fig. 5 (vi).

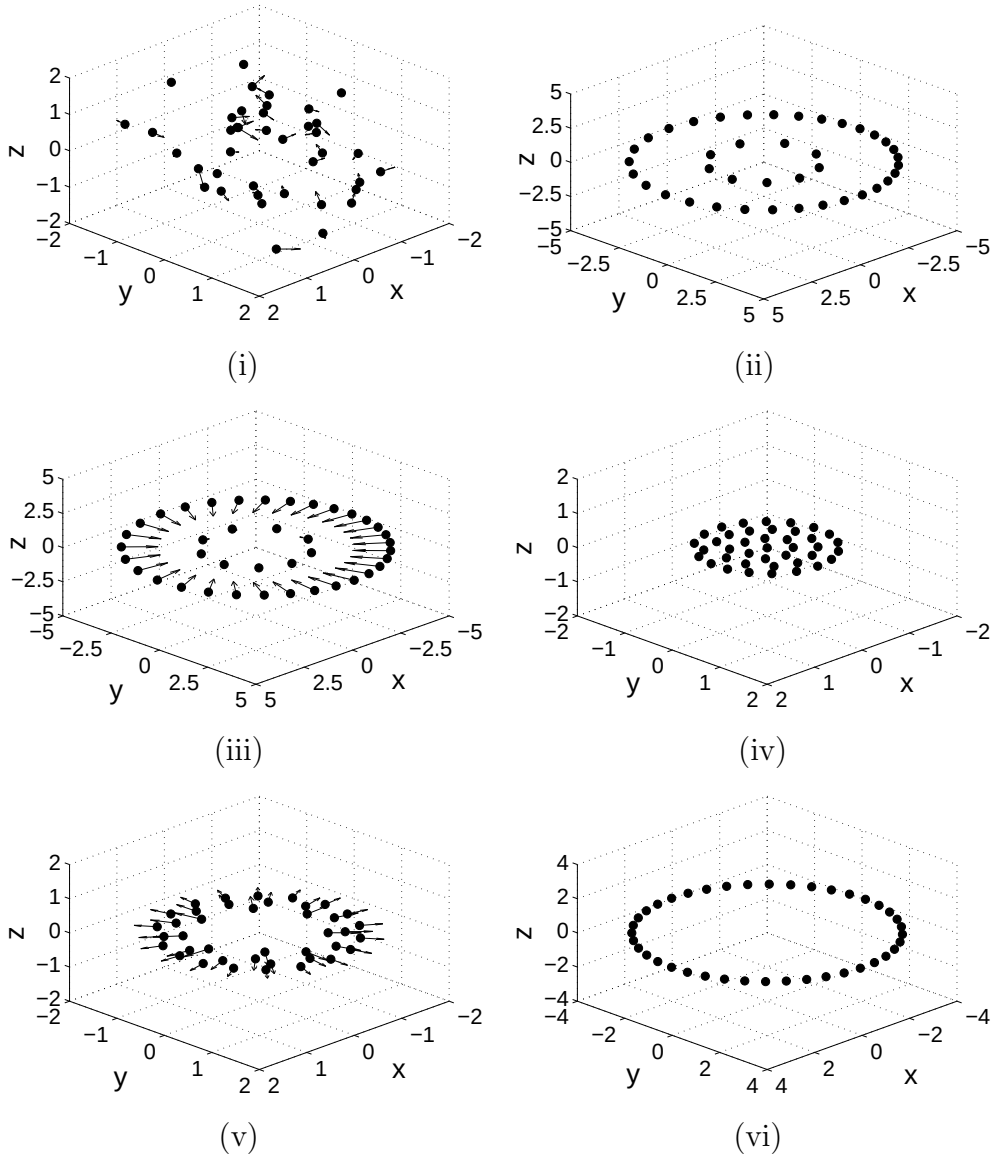

Figure 5: Pitchfork bifurcation (i) random initial conditions (ii) double ring ($\mu = 2, r = 3.5, t = 19s$) (iii) bifurcation of the system ($\mu = -5, r = 0, t = 20s$) (iv) cluster ($t = 39s$) (v) bifurcation of the system ($\mu = -5, r = 4, t = 40s$) (vi) ring, radius = 4, ($t = 60s$)

4. APPLICATION

The purpose of the previous sections was to demonstrate how classical static bifurcations can be used to steer a formation of spacecraft, allowing for a simple transition between formations. To ensure the stability for real, safety or mission critical systems this new approach will be extended to consider actuator saturation and communication limitations.

4.1. Actuator Saturation

From Eq. 2 the control force, $\mathbf{u}_i$, acting on each spacecraft is

$$\mathbf{u}_i = \mathbf{u}^S + \mathbf{u}^R + \mathbf{u}^d \tag{45}$$

where,

$$\begin{pmatrix} \mathbf{u}^S \\ \mathbf{u}^R \\ \mathbf{u}^d \end{pmatrix} = \begin{pmatrix} -\nabla_i U^S(\mathbf{x}_i) \\ -\nabla_i U^R(\mathbf{x}_{ij}) \\ -\sigma \mathbf{v}_i \end{pmatrix} \tag{46}$$

From the triangle inequality [23] the maximum control force must then be

$$|\mathbf{u}_i| \leqslant |\nabla_i U^S(\mathbf{x}_i)| + |\nabla_i U^R(\mathbf{x}_{ij})| + |\sigma \mathbf{v}_i| \tag{47}$$

The maximum control force that the system is required to produce will therefore be dependent upon the sum of the maximum gradient of the *Steering* and *Repulsive Potential* and the maximum speed that each spacecraft can move.

Considering the classical pitchfork bifurcation as the *Steering Potential*, referring back to Eq. 20, it can be seen that the control force is unbound as the distance ρ_i from the origin increases. To overcome this Badawy and McInnes [2] have devised a promising approach through the use of hyperbolic potential functions. This function has a smooth shape at the goal state whilst becoming asymptotic with a constant gradient (thus bounded control force) as the distance from origin increases. Equation 48 and Fig. 6 show the hyperbolic control potential, $U_h(\rho_i)$, that can be used as the *Steering Potential* in order to achieve a bounded control force.

$$U_h(\rho_i) = C_h \left[(\rho_i - r)^2 + 1 \right]^{0.5} \tag{48}$$

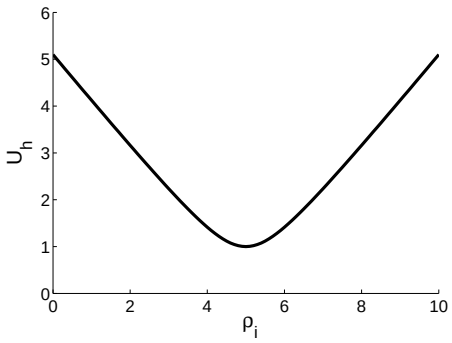

Figure 6: Hyperbolic Potential Function ($C_h = 1$, $r = 5$)

where C_h controls the amplitude of the function.

To make use of the principles demonstrated through the static bifurcations an additional exponential potential function, $U_e(\rho_i)$, is added, as shown in Eq. 49 and Fig. 7.

$$U_e(\rho_i) = \mu C_e \exp^{-(\rho_i - r)^2 / L_e} \tag{49}$$

where C_e and L_e represent the amplitude and length-scale of the function respectively and μ is the bifurcation parameter.

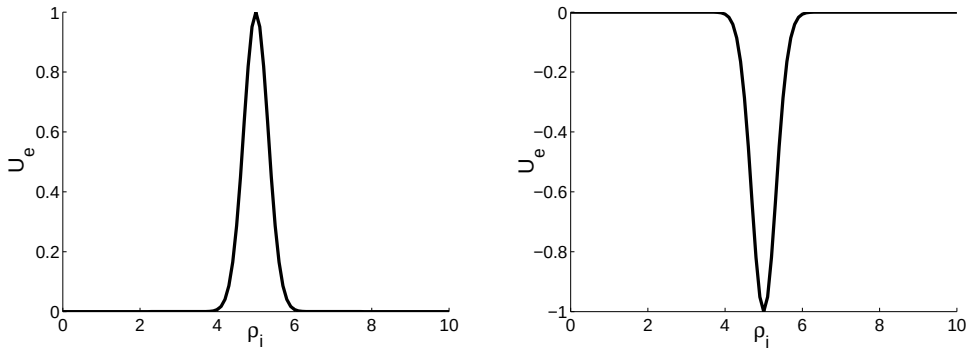

(i) (ii)

Figure 7: Exponential potential function ($C_e = 1$, $L_e = 1$, $r = 5$): (i) $\mu > 0$ (ii) $\mu < 0$

Combining Eq. 48 and 49 forms the new *Steering Potential* equation as shown in Eq. 50 and Fig. 8. If the bifurcation parameter $\mu < 0$ there is one goal state, as shown in Fig. 8 (i). If however, the system is bifurcated such

that $\mu > 0$ the system splits into a state with two stable goal positions as shown. The last term in Eq. 50 ensures that the formation is created in the x-y plane, as shown in Fig. 8 (ii).

$$\begin{aligned} U^S(\mathbf{x}_i) &= U_h(\rho_i) + U_e(\rho_i) + U_h(z_i) \\ &= C_h \left[(\rho_i - r)^2 + 1\right]^{0.5} + \mu C_e \exp^{-(\rho_i - r)^2/L_e} + C_z \left[z_i^2 + 1\right]^{0.5} \end{aligned} \quad (50)$$

where the constant C_z controls the amplitude of this bound hyperbolic potential function.

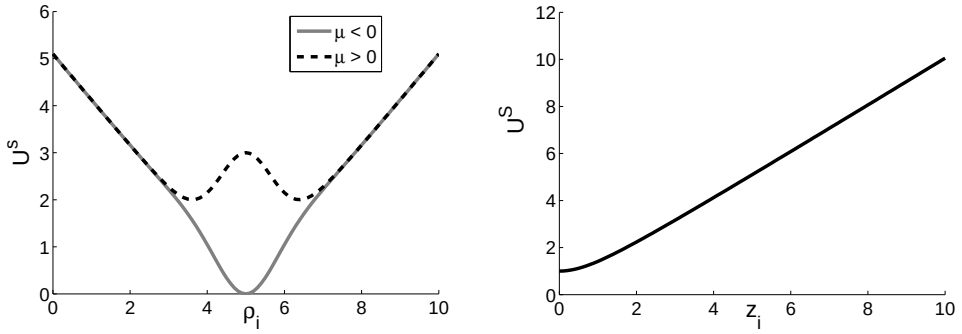

(i) (ii)

Figure 8: *Steering Potential* Function: (i) U_h^S, $\mu < 0$ ($C_h = 1$, $C_e = 1$, $L_e = 1$, $r = 5$) (ii) U_h^S, $\mu > 0$ ($C_h = 1$, $C_e = 3$, $L_e = 1$, $r = 5$) (iii) U_z^S ($C_z = 1$)

As the purpose of the new *Steering Potential* is to have a bounded control force it is important to determine the maximum control force for the hyperbolic and exponential potential functions in order to place a bound on the *Steering Potential*. Considering the hyperbolic function, the control force, $\mathbf{u}_h$, is shown in Eq. 51 and Fig. 9

$$\mathbf{u}_h = -\nabla_i U_h(\rho_i, z_i) = \left[-\frac{C_h(\rho_i - r)}{\left[(\rho_i - r)^2 + 1\right]^{0.5}}, -\frac{C_z z_i}{(z_i^2 + 1)^{0.5}} \right]^T \quad (51)$$

Therefore, as $\rho_i \to \infty$, $\mathbf{u}_h \to -C_h$; $\rho_i \to 0$, $\mathbf{u}_h \to C_h$ and as $z_i \to \infty$, $\mathbf{u}_z \to -C_z$ as shown in Fig. 9.

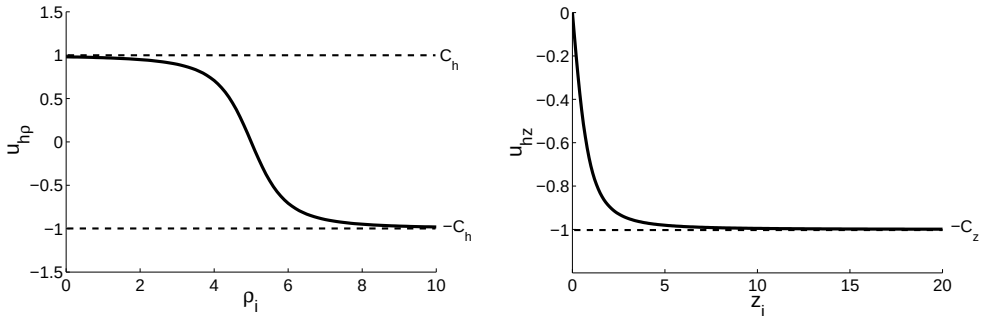

Figure 9: Hyperbolic Control Force: (i) ρ_i direction ($C_h = 1$) (ii) z_i direction ($C_z = 1$)

The exponential control force can be defined as

$$\mathbf{u}_e = -\nabla_i U_e(\rho_i, z_i) = \left[2\mu \frac{C_e}{L_e}(\rho_i - r)\exp^{-(\rho_i - r)^2/L_e}, 0\right]^T \tag{52}$$

The maximum exponential control forces occurs when $\rho_i = r \pm \sqrt{\frac{L_e}{2}}$ giving the maximum control force, $\mathbf{u}_e$, equal to $\pm\sqrt{2}\mu \exp^{-0.5}\frac{C_e}{\sqrt{L_e}}$ as shown in Fig. 10.

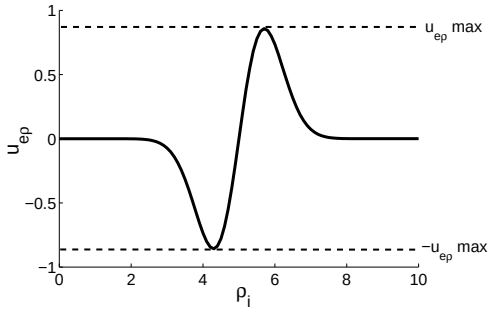

Figure 10: Exponential Control Force ($\mu = 1$, $C_e = 1$ and $L_e = 1$)

Therefore, depending upon the constants chosen in the equations the maximum bounded control force in the ρ_i direction will either be controlled through the hyperbolic or exponential term in the *Steering Potential* equation. The equations have to be evaluated to determine if either the hyperbolic or exponential term dominates as shown in Fig. 11 (i) and (ii). Considering

the case when $\mu > 0$ with constants choosen so that the hyperbolic term dominates then, $|\nabla_i U^S(\rho_i)|_{max} = C_h$. If, however, the exponential term dominates then $|\nabla_i U^S(\rho_i)|_{max}$ can be found numerically. In the z direction, $|\nabla_i U^S(z_i)|_{max} = C_z$ as shown in Fig. 9 (ii).

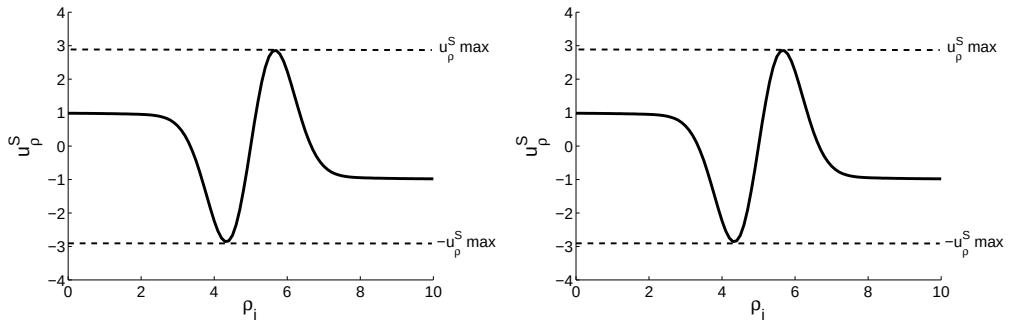

Figure 11: *Steering Potential* Control Force: (i) $\mathbf{u}_h$ dominating (ii) $\mathbf{u}_e$ dominating

The bound *Steering Potential* control force is then

$$|\mathbf{u}^S| = |\nabla_i U^S(\mathbf{x}_i)|_{max} \leq \left[\left(\nabla_i U^S(\rho_i)_{max} \right)^2 + \left(\nabla_i U^S(z_i)_{max} \right)^2 \right]^{0.5} \tag{53}$$

The *Repulsive Potential* is a bound force that has a maximum value equal to C_R/L_R that occurs when $\mathbf{x}_{ij} = 0$. This would, however, occur when two spacecraft are in the same position and therefore would have collided. The realistic maximum control force would therefore be $(\mathbf{u}_i^R)_{max} = C_R/L_R \exp^{-(|\mathbf{x}_{ij}|_{min}/L_R)}$ where, $|\mathbf{x}_{ij}|_{min} = |\mathbf{x}_i - \mathbf{x}_j|_{min}$, is the minimum separation distance between both spacecraft without colliding as shown in Fig. 12 (ii) for example.

The maximum control force is therefore

$$|\mathbf{u}^R| = |\nabla_i U^R(\mathbf{x}_{ij})|_{max} = \frac{C_r}{L_r} \exp^{-|\mathbf{x}_{ij}|_{min}/L_r} \tag{54}$$

where $|\mathbf{x}_{ij}|_{min} = L_r \ln \left(\dfrac{2C_r}{mV_m^2} \right)$ and V_m is the maximum speed of the spacecraft.

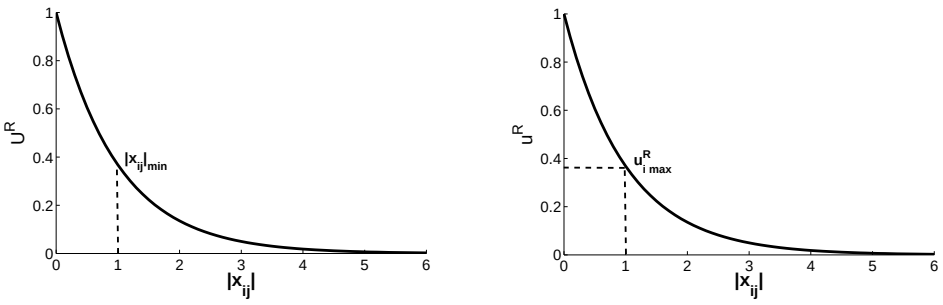

(i) (ii)

Figure 12: *Repulsive Potential*: (i) potential function (ii) control force

The dissipative force, $\mathbf{u}^d$ is bound by the maximum speed as follows

$$|\mathbf{u}^d| = |\sigma \mathbf{v}_i|_{max} \leq \sigma V_m \tag{55}$$

The maximum total force that the actuator will generate is therefore,

$$|\mathbf{u}_i| \leqslant |\nabla_i U^S(\mathbf{x}_i)| + |\nabla_i U^R(\mathbf{x}_{ij})| + |\sigma \mathbf{v}_i| \tag{56}$$

If the *Steering Potential* is dominated by the hyperbolic term, the maximum control force is

$$\begin{aligned} |\mathbf{u}_i| &\leqslant |\nabla_i U^S(\mathbf{x}_i)| + |\nabla_i U^R(\mathbf{x}_{ij})| + |\sigma \mathbf{v}_i| \\ &\leqslant \sqrt{C_h^2 + C_z^2} + \frac{C_r}{L_r} \exp^{-|\mathbf{x}_{ij}|_{min}/L_r} + \sigma V_m \end{aligned} \tag{57}$$

If, however, the *Steering Potential* is dominated by the exponential term, $|\nabla_i U^S(\mathbf{x}_i)|$ will have to be evaluated with $|\nabla_i U^S(z_i)_{max}| = C_z$, $|\nabla_i U^R(\mathbf{x}_{ij})| = \frac{C_r}{L_r} \exp^{-|\mathbf{x}_{ij}|_{min}/L_r}$ and $|\sigma \mathbf{v}_i| = \sigma V_m$.

5. Sensing Region

Although the artificial potential function method is theoretically elegant, Sigurd points out that the assumption that all spacecraft in a swarm have information on all other spacecraft is unrealistic as the number of spacecraft increase [31]. To address this issue each spacecraft will now have a sensing

region [18, 9, 22] that will ensure collision avoidance and an equally spaced final formation, as shown in Eq. 58 and Fig. 13.

$$U_{ij}^{R} = \left\{ \begin{array}{ll} \sum_{j,j\neq i} C_r \exp^{-|\mathbf{x}_{ij}|/L_r} & \text{if } |\mathbf{x}_{ij}| \leq Z_r \\ 0 & \text{if } |\mathbf{x}_{ij}| > Z_r \end{array} \right\} \tag{58}$$

where Z_r is the radius of repulsive zone of influence.

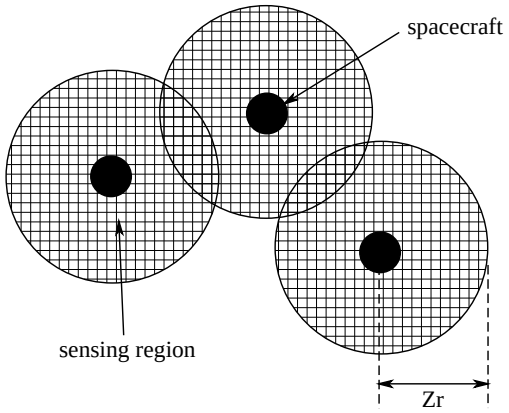

Figure 13: Spacecraft *Repulsive Potential* sensing region

Therefore, as the *Repulsive Potential* only acts in a region surrounding each spacecraft, scale separation will still hold true so that the system will move under the influence of a long-range *Steering Potential* but with short-range collision avoidance. While not a rigorous proof, related work by Tanner has shown that, by using graph theory, if the communication network between the spacecraft remains connected for all time the system is guaranteed to relax into the minimum of the potential [33].

5.1. Relative Motion Dynamics

In this section the swarm model discussed in the previous section will be adapted to consider gravitational effects, demonstrating SFF in a simplified low-Earth-orbit model. Initially, consider the relative motion dynamics of two spacecraft, in close proximity, traveling around a spherical Earth [5]. It is assumed that the target spacecraft is in a circular orbit around the Earth with an orbital radius R_t and orbital rate $\omega_e = \sqrt{\mu_g/R_t^3}$, as summarised in

Fig. 14.

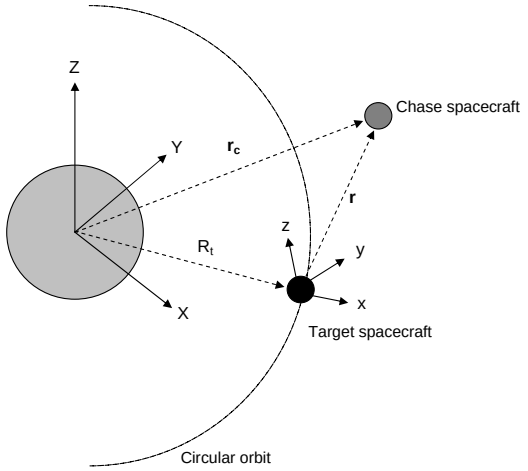

Figure 14: Motion of spacecraft orbiting the Earth

Assuming that there are no external forces or disturbances acting on each spacecraft and letting the position of the chase spacecraft relative to the target spacecraft be $\mathbf{r}$, then the motion in the Earth-centered reference frame for the target and chase spacecraft [32] is

$$\ddot{\mathbf{r}}_t + \frac{\mu}{|\mathbf{r}_t|^3}\mathbf{r}_t = 0 \tag{59}$$

$$\ddot{\mathbf{r}}_c + \frac{\mu}{|\mathbf{r}_c|^3}\mathbf{r}_c = 0 \tag{60}$$

where $|\mathbf{r}_t| = R_t$ and $|\mathbf{r}_c| = \left[(R_t + x)^2 + y^2 + z^2\right]^{0.5}$.

Taking the difference between the equations of motion of the chase and target spacecraft results in

$$\ddot{\mathbf{r}} + \frac{\mu}{|\mathbf{r}_t + \mathbf{r}|^3}(\mathbf{r}_t + \mathbf{r}) - \frac{\mu}{|\mathbf{r}_t|^3}\mathbf{r}_t = 0 \tag{61}$$

where $\mathbf{r} = \mathbf{r}_c - \mathbf{r}_t$.

Assuming that the orbital radius of the target spacecraft is much larger than the relative distance between the spacecraft ($|\mathbf{r}_t| >> |\mathbf{r}|$), the non-linear

relative equations of motion can be linearised to form the Clohessy-Wiltshire or Hill's (HCW) relative equations of motion, in the Local Vertical Local Horizontal (LVLH) frame attached to the target spacecraft, as follows

$$\ddot{x} - 2\omega_e \dot{y} - 3\omega_e^2 x = 0 \tag{62}$$

$$\ddot{y} + 2\omega_e \dot{x} = 0 \tag{63}$$

$$\ddot{z} + \omega_e^2 z = 0 \tag{64}$$

The closed form solutions of the HCW equations are given by Eq. 65-67 [32].

$$x(t) = \frac{\dot{x}_0}{\omega_e}\sin(\omega_e t) - \left(3x_0 + \frac{2\dot{y}_0}{\omega_e}\right)\cos(\omega_e t) + \left(4x_0 + \frac{2\dot{y}_0}{\omega_e}\right) \tag{65}$$

$$y(t) = \frac{2\dot{x}_0}{\omega_e}\cos(\omega_e t) + \left(6x_0 + \frac{4\dot{y}_0}{\omega_e}\right)\sin(\omega_e t) - (6\omega_e x_0 + 3\dot{y}_0)t - \frac{2\dot{x}_0}{\omega_e} + y_0 \tag{66}$$

$$z(t) = \frac{\dot{z}_0}{\omega_e}\sin(\omega_e t) + z_0\cos(\omega_e t) \tag{67}$$

where $[x_o, y_o, z_o]^T$ and $[\dot{x}_o, \dot{y}_o, \dot{z}_o]^T$ are the position and velocity initial conditions at $t = 0$ respectively.

From Eq. 66 it can be seen that the 3rd term of $y(t)$ becomes unbound with time, so that if the constraint $2\omega_e x_0 + \dot{y}_0 = 0$ is satisfied, it will ensure that the chase spacecraft does not drift away from the leader. Using this constraint the HCW admit periodic solutions given by Eq. 68 [34]

$$\begin{bmatrix} x \\ y \\ z \\ \dot{x} \\ \dot{y} \\ \dot{z} \end{bmatrix} = \begin{bmatrix} \frac{c_1}{2}\sin(\omega_e t + \alpha_o) \\ c_1\cos(\omega_e t + \alpha_0) + c_3 \\ c_2\sin(\omega_e t + \beta_0) \\ \frac{c_1}{2}\omega_e\cos(\omega_e t + \alpha_o) \\ -c_1\omega_e\sin(\omega_e t + \alpha_0) \\ c_2\omega_e\cos(\omega_e t + \beta_0) \end{bmatrix} \tag{68}$$

where $c_1, c_2, c_3, c_4, \alpha_0$ and β_0 are constant, determined from the initial conditions.

Depending upon the choice of free-parameters, c_1, c_2, c_3, α_0 and β_0, a variety of bounded relative orbits can be achieved. Orbits known as projected circular orbits (PCO) can be achieved by choosing $c_1, c_2 = \rho_c$, $c_3 = 0$ and $\alpha_0 = \beta_0$ so that the relative orbit of the chase spacecraft in the $y - z$ plane is circular with radius, ρ_c. The initial conditions are then

$$\begin{bmatrix} x_0 \\ y_0 \\ z_0 \\ \dot{x}_0 \\ \dot{y}_0 \\ \dot{z}_0 \end{bmatrix} = \begin{bmatrix} \frac{\rho_c}{2}\sin(\alpha_0) \\ \rho_c \cos(\alpha_0) \\ \rho_c \sin(\alpha_0) \\ \frac{\rho_c}{2}\omega_e \cos(\alpha_0) \\ -\rho_c \omega_e \sin(\alpha_0) \\ \rho_c \omega_e \cos(\alpha_0) \end{bmatrix} \tag{69}$$

so that

$$y^2 + z^2 = \rho_c^2 \tag{70}$$

As an example, consider the case where it is desired that the chase spacecraft be in a PCO, $\rho_c = 1000$ m in the $y - z$ plane, about the target spacecraft orbiting at a radius, $R_t = 6671$ km (300 km above the Earth's surface). Therefore, the initial conditions for the chase spacecraft are as follows

$$\begin{bmatrix} x_o \\ y_o \\ z_o \\ \dot{x}_o \\ \dot{y}_o \\ \dot{z}_o \end{bmatrix} = \begin{bmatrix} 0 \\ -1000 \text{ m} \\ 0 \\ -0.5795 \text{ ms}^{-1} \\ 0 \\ -1.1590 \text{ ms}^{-1} \end{bmatrix} \tag{71}$$

where $\alpha_0 = 180^o$.

Figure 15 (i) shows the motion of the chase spacecraft relative to the target spacecraft in the LVLH frame, with Fig. 15 (ii) showing the projection of the spatial orbit onto the $y - z$ plane. As can be seen from the results,

the chase spacecraft achieves the desired bound circular periodic orbit in the $y - z$ plane with radius, $\rho_c = 1000$ m.

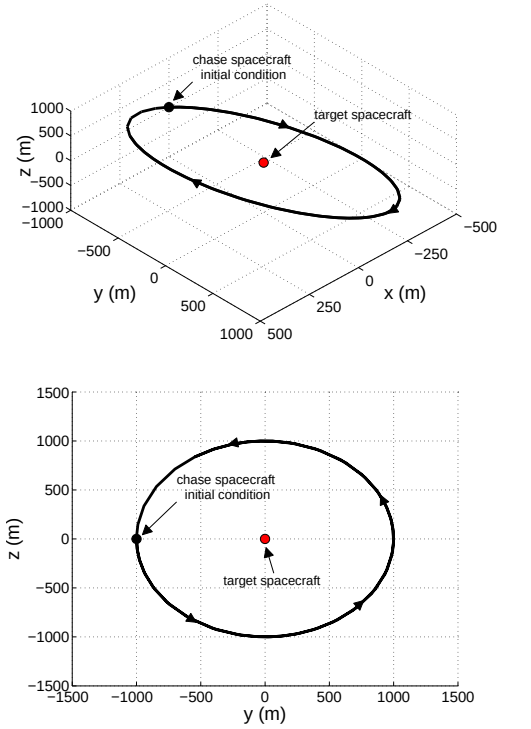

(i) (ii)

Figure 15: Motion of the chase spacecraft relative to the target spacecraft (i) $x - y - z$ plane (ii) $y - z$ plane

Therefore, it has been shown that if the initial conditions of a spacecraft are choosen to satisfy the PCO initial conditions, then a spacecraft can follow a circular periodic orbit about a target spacecraft. The bifurcating potential field will now be used to force a swarm of spacecraft onto a desired equally spaced PCO from arbitrary initial conditions and then bifurcate to a different equally spaced periodic orbit. To force the spacecraft onto a desired orbit with radius, ρ_c, in the $y - z$ plane, the following *Steering Potential* will be used

$$U^S(\mathbf{x}_i) = C_x \left[(x_i - \frac{\rho_c}{2})^2 + 1\right]^{0.5} + C_h \left[(\rho_{yz} - \rho_c)^2 + 1\right]^{0.5} + \mu C_e \exp^{-(\rho_{yz}-\rho_c)^2/L_e} \tag{72}$$

where $\rho_{yz} = (y_i^2 + z_i^2)^{0.5}$.

From Eq. 69 it is known that the desired velocity of the spacecraft to orbit on the PCO is a function of α_0, ρ_c and ω_e, so that if the spacecraft were to start far from the desired PCO, a simple first order controller could be used to drive the system to the desired velocity, with the *Steering Potential* forcing the system to the desired orbit. The HCW equations of motion given in Eq. 62-64 are re-cast into the swarm model, including the new forcing terms as follows

$$\ddot{x}_i - 2\omega_e \dot{y}_i - 3\omega_e^2 x_i = -\frac{\partial U^R}{\partial x_i} - \frac{\partial U^S}{\partial x_i} - \lambda_v (\dot{x}_i - \dot{x}_d) \tag{73}$$

$$\ddot{y}_i + 2\omega_e \dot{x}_i = -\frac{\partial U^R}{\partial y_i} - \frac{\partial U^S}{\partial y_i} - \lambda_v (\dot{y}_i - \dot{y}_d) \tag{74}$$

$$\ddot{z}_i + \omega_e^2 z_i = -\frac{\partial U^R}{\partial z_i} - \frac{\partial U^S}{\partial z_i} - \lambda_v (\dot{z}_i - \dot{z}_d) \tag{75}$$

where $\dot{x}_d = \frac{\rho_c}{2}\omega_e \cos(\alpha_0)$, $\dot{y}_d = -\rho_c \omega_e \sin(\alpha_0)$, $\dot{z}_d = \rho_c \omega_e \cos(\alpha_0)$ and λ_v is an inverse time constant determining the response of the system.

Consider a formation of 5 spacecraft that have mass 10 kg and minimum separation distance, $|\mathbf{x}_{ij}|_{min} = 3$ m, that are required to achieve three different PCOs with radius of 5 m, 10 m and 15 m. Each spacecraft are given random initial positions (satisfying the constraint that $|\mathbf{x}_{ij}|_{initial} > 3$ m), with an initial maximum speed of 0.1 ms^{-1}, sensing radius, $Z_r = 10$ m and maximum actuator force of 2 N. To satisfy these conditions, Table 2 summarises the bound potential constants used in each formation.

From **Section 4.1**, the maximum bounded control force from Eq. 73-75 can be estimated as

$$|\mathbf{u}^S| = |\nabla_i U^S(\mathbf{x}_i)|_{max} = \sqrt{(C_x^2 + C_h^2)} \tag{76}$$

Table 2: LEO SFF bound constants

Formation	μ	ρ_c	C_h	C_x	C_e	L_e	C_r	L_r	λ_v
A	0	5	0.3	0.3	-	-	4	0.8	10
B	0	10	0.3	0.3	-	-	4	2	10
C	0	15	0.3	0.3	-	-	4	3	10

$$|\mathbf{u}^R| = |\nabla_i U^R(\mathbf{x}_{ij})|_{max} = \frac{C_r}{L_r} \exp^{-|\mathbf{x}_{ij}|_{min}/L_r} \tag{77}$$

$$|\mathbf{u}^d| = |\lambda_v(\dot{\mathbf{x}}_i - \dot{\mathbf{x}}_d)|_{max} = \lambda_v(|\dot{\mathbf{x}}|_{max} - |\dot{\mathbf{x}}_d|_{min}) = \lambda_v(|\dot{\mathbf{x}}|_{max} - \rho_c\omega_e) \tag{78}$$

The results of the simulation are shown in Fig. 16-18 indicating that the formation of spacecraft can successfully create desired patterns and autonomously reconfigure between them.

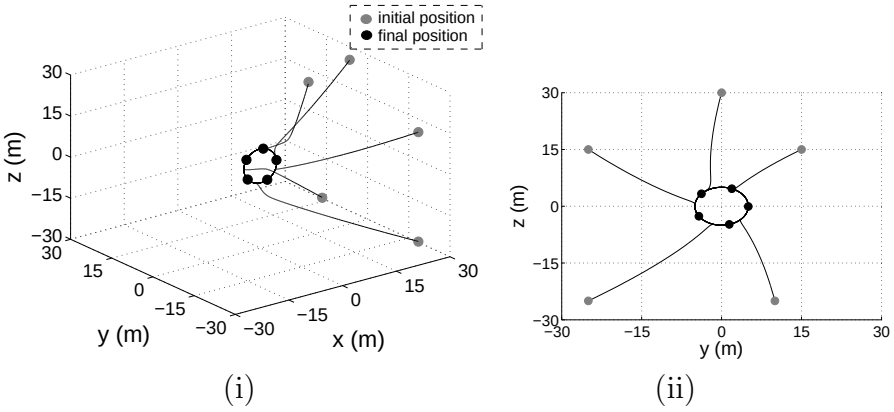

(i) (ii)

Figure 16: Formation A - $\rho_{ca} = 5$ m (i) $x - y - z$ plane (ii) $y - z$ plane

Figure 19 confirms that the desired PCO are achieved in each formation and that collision avoidance is ensured throughout the simulation.

Figure 20 shows the velocity profile of each spacecraft in the x, y and z directions, with the results showing that the swarm of spacecraft are successfully driven to the desired velocity once in the equilibrium formation.

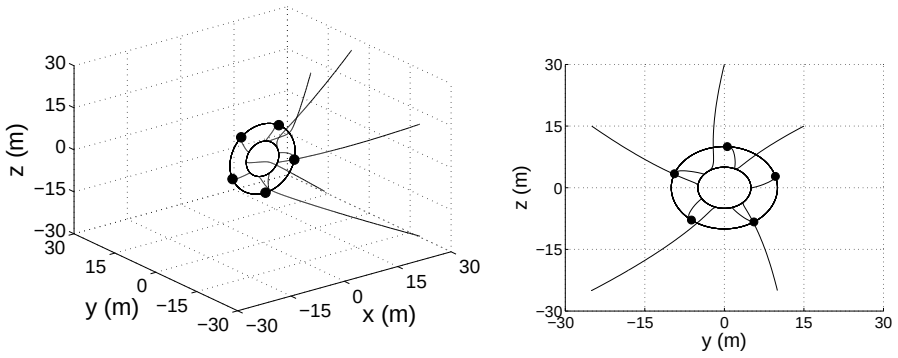

(i) (ii)

Figure 17: Formation B - $\rho_{cb} = 10$ m (i) $x - y - z$ plane (ii) $y - z$ plane

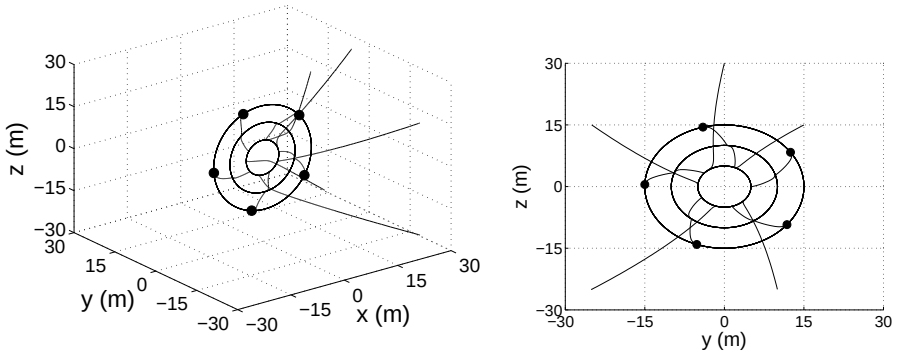

(i) (ii)

Figure 18: Formation C - $\rho_{cc} = 15$ m (i) $x - y - z$ plane (ii) $y - z$ plane

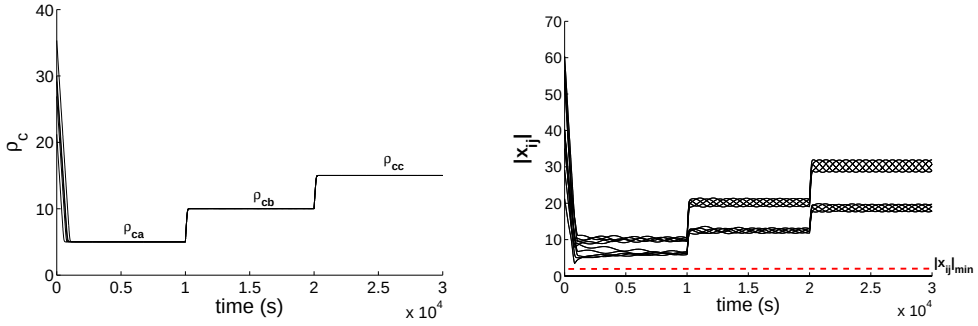

(i) (ii)

Figure 19: Formation A, B and C (i) relative orbit radius (ii) separation distance

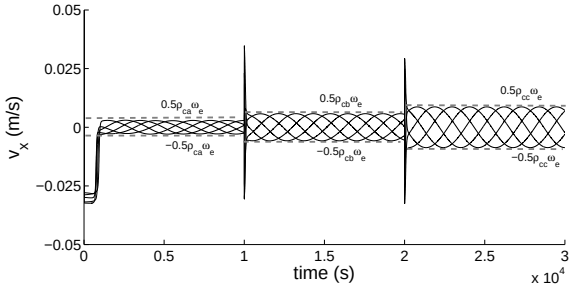

(i)

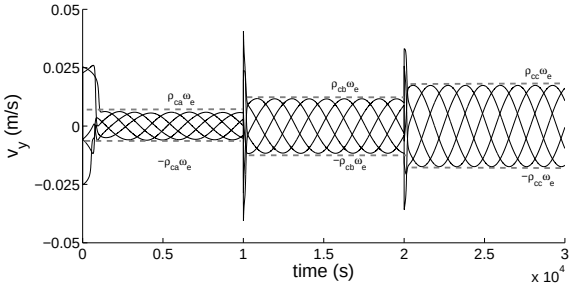

(ii)

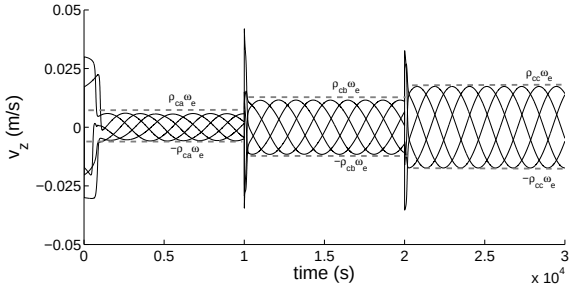

(iii)

Figure 20: Formation velocity (i) v_x (ii) v_y (iii) v_z

Figure 21 shows the actuator force acting on each spacecraft. As expected the largest force occurs at the beginning of each formation, driving each spacecraft to the desired PCO. Once in this condition the actuator force decays to zero and the swarm of spacecraft follows an equally spaced periodic orbit. Table 3 shows that the simulated swarm actuator force is lower than the analytical bound force satisfying the constraint that the actuator force should be less than 2 N.

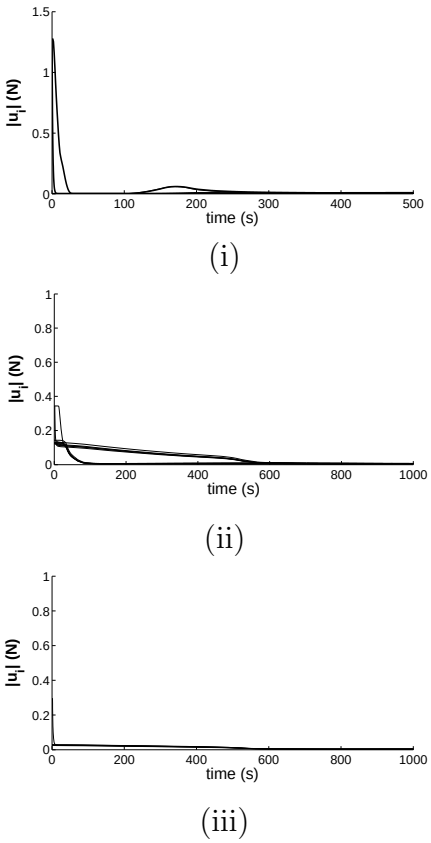

Figure 21: Actuator force (i) formation A (ii) formation B (iii) formation C

Table 3: LEO SFF control force

Formation	Analytical $\|\mathbf{u}_i\|_{max}$ (N)	Simulated $\|\mathbf{u}_i\|_{max}$ (N)
A	1.4	1.3
B	1.3	0.3
C	1.2	0.3

This section has considered the implementation of the bifurcating SFF model in LEO orbit, taking advantage of the HCW linear, unperturbed equations of relative motion that yield closed periodic solutions. It was shown that using the bound bifurcating swarm potentials, that a swarm of spacecraft can be driven safely towards a desired periodic orbit, relaxing into an equally spaced rotating ring formation about a target spacecraft. Potential applications of these formations include simultaneous scientific data gathering that could be used to forecast weather or make gravity field measurements, with the swarm being able to reconfigure to meet different mission requirements.

The linear, unperturbed HCW equations of motion provide a starting point to demonstrate the implementation of the swarm model for SFF in LEO. There are, however, several real world non-linear effects that can be considered to improve the model. For example, higher order orbital dynamics will include significant perturbations such as the Earth gravity harmonics. The largest of these is the second zonal harmonic J_2 perturbation, which is caused by the oblateness of the Earth [30]. Other perturbations include drag, solar radiation and the eccentricity of the reference orbit [27, 11]. Also, as there was no consideration to the form of propulsion used it was assumed that the spacecraft could move instantaneously in all degrees-of-freedom and that each spacecraft could sense other spacecraft in close proximity. Finally, although the method is not fuel optimal it is seen as an effective means of controlling complex reformation manoeuvres only, with station-keeping between the manoeuvres using classical optimal control methods.

6. Conclusion

It has been shown that by using the new approach of bifurcating artificial potential fields SFF can be achieved. Through a simple parameter change to the potential this approach allows a system of spacecraft to autonomously

form different formations. An important step in real engineered systems is to ensure that the formation can form reliably. Through dynamical systems theory the stability of the SFF model was investigated analytically to ensure that desired behaviours will always occur. Practical considerations such as the issue of actuator saturation and communication limitations are addressed, developing a new bounded control force model based on the principles of classical bifurcating potential fields. To demonstrate this the SFF model was adapted to consider gravitational effects in low-Earth-orbit, utilising the Clohessy-Wiltshire relative linearised equations of motion. It was shown that a formation of spacecraft can be driven safely onto equally spaced projected circular orbits, autonomously reconfiguring between them, whilst satisfying constraints made regarding each spacecraft.

References

[1] A. Badawy, On-Orbit Manoeuvring Using Superquadric Potential Fields, Ph.D. thesis, University of Strathclyde, 2007.

[2] A. Badawy, C. McInnes, On-orbit assembly using superquadric potential fields, Journal of Guidance, Control, and Dynamics 31 (2008) 30–43.

[3] F. Bauer, J. Bristow, D. Folta, K. Hartman, D. Quinn, J. Howt, Satellite formation flying using an innovative autonomous control system (autocon) environment, in: AIAA Guidance, Navigation, and Control Conference, New Orleans, USA, pp. 657–666.

[4] C. Bender, S.A. Orszag, Advanced Mathematical Methods for Scientists and Engineers: Asymptotic Methods and Perturbation Theory, Springer, 1978.

[5] W. Bong, Space Vehicle Dynamics and Control, American Institute of Aeronautics and Astronautics, Reston, VA, 2nd edition, 2008.

[6] K. Carpenter, C. Schrijver, R. Allen, A. Brown, D. Chenette, W. Danchi, M. Karovska, S. Kilston, R. Lyon, J. Marzouk, L. Mazzuca, R. Moe, F. Walter, N. Murphy, The stellar imager (SI): a revolutionary large-baseline imaging interferometer at the Sun-Earth L_2 point, New Frontiers in Stellar Interferometry 5491 (2004) 243–254.

[7] K. Do, J. Pan, Non-linear formation control of unicycle-type mobile robots, Robotics and Autonomous Systems 55 (2007) 191–204.

[8] M. D'Orsogna, Y. Chuang, A. Bertozzi, S. Chayes, The road to catastrophe: Stability and collapse in 2D driven particle systems, in: Hawaii International Conference on Statistics, Mathematics and Related Fields, Honolulu, Hawaii, USA.

[9] S. Ge, Y. Cui, Dynamic motion planning for mobile robots using potential field method, Autonomous Robots 13 (2002) 207–222.

[10] E. Gill, M. Steckling, P. Butz, Gemini: A milestone towards autonomous formation flying, in: ESTEC, ESA Workshop on On-Board Autonomy, Noordwijk, Netherlands.

[11] A. Golikov, Evolution of formation flying satellite relative motion: Analysis based on the theona satellite theory, in: Proceedings of the 17th International Symposium on Space Flight Dynamics, Moscow, Russia.

[12] E. Grøtli, Modeling and Control of Formation Flying Satellites in 6 DOF, Ph.D. thesis, Norwegian University of Science and Technology, 2005.

[13] D. Izzo, L. Pettazi, Autonomous and distributed motion planning for satellite swarm, Journal of Guidance, Control, and Dynamics 30 (2007) 449–459.

[14] P. Jones, M. Blake, J. Archibald, A real-time algorithm for task allocation, in: International Symposium on Intelligent Control, Vancouver, Canada, pp. 672–677.

[15] D. Jordon, P. Smith, Nonlinear Ordinary Differential Equations: An Introduction to Dynamical Systems, Oxford University Press, 1999.

[16] J. LaSalle, An invariance principle in the theory of stability, International Symposium on Differential Equations and Dynamical Systems (1967) 277–286. Ed. New York: Academic Press.

[17] J. Lawton, A behavior-based approach to multiple spacecraft formation flying, Ph.D. thesis, Brigham Young University, 2000.

[18] N. Leonard, E. Fiorelli, Virtual leaders, artificial potentials and coordinated control of groups, in: Proceedings of the 40th IEEE Conference on Decision and Control, volume 3, Orlando, FL, USA, pp. 2968–2973.

[19] C. McInnes, Vortex formation in swarms of interacting particles, Physical Review E 75 (2007) 032904.

[20] C.R. McInnes, Autonomous ring formation for a planar constellation of satellites, Journal Guidance, Control and Dynamics 18 (1995) 1215–1217.

[21] F. McQuade, Autonomous Control for On-orbit Assembly using Artificial Potential Functions, Ph.D. thesis, University of Glasgow, 1997.

[22] P. Ogren, E. Fiorelli, N. Leonard, Cooperative control of mobile sensor networks: Adaptive gradient climbing in a distributed environment, IEEE Transactions on Automatic Control 49 (2004) 1292–1302.

[23] L. Rade, B. Westergren, Mathematics Handbook for Science and Engineering, Studentlitteratur, 1989.

[24] J. Reif, H. Wang, Social potential fields: A distributed behavioral control for autonomous robots, Robots and Autonomous Systems 27 (1999) 171–194.

[25] W. Ren, R. Beard, A decentralized scheme for spacecraft formation flying via the virtual structure approach, in: Proceedings of the American Control Conference, Denver, Colorado, USA, pp. 1747–1751.

[26] J. Roberts, Satellite formation flying for an interferometry mission, Ph.D. thesis, Cranfield University, 2005.

[27] C. Sabol, R. Burns, C. McLaughlin, Satellite formation flying design and evolution, Journal of Spacecraft and Rockets 38 (2001) 270–278.

[28] D. Scharf, F. Hadaegh, S. Ploen, A survey of spacecraft formation flying guidance and control (Part II): Control, in: American Control Conference, Colorado, US, pp. 2976–2985.

[29] D. Scharf, F. Hadaegh, S. Ploen, Precision formation delta-v requirements for distributed platforms in Earth orbit, in: SPIE Remote Sensing of the Atmosphere, Ocean, Environment, and Space Conference, Honolul, Hawaii, USA.

[30] H. Schaub, K. Alfriend, J_2 invariant relative orbits for spacecraft formations, in: Celestial Mechanics and Dynamical Astronomy, volume 79, Springer Netherlands, 2001.

[31] K. Sigurd, H. J, UAV trajectory design using total field collision avoidance, in: AIAA Guidance, Navigation and Control Conference, Austin, Texas, USA.

[32] A. Sparks, Satellite formation keeping control in the presence of gravity perturbations, in: Proceedings of the American Control Conference, Chicago, Illinois, USA.

[33] H. Tanner, A. Jadbabaie, G. Pappas, Flocking in fixed and switching networks, IEEE Transactions on Automatic Control 52 (2007) 863–868.

[34] V. Vaddi, Modelling and control of satellite formations, Ph.D. thesis, Texas A and M University, 2003.

[35] O. Wallner, Darwin system assessment study, Astrium Summary Report, European Space Agency 1 (2006) 1–18.

[36] P. Wang, F. Hadaegh, Coordination and control of multiple microspacecraft moving in formation, Journal of the Astronautical Sciences 44 (1996) 315–355.

[37] A. Winfield, C. Harper, J. Nembrini, Towards dependable swarms and a new discipline of swarm engineering, in: E. Sahin, W. Spears (Eds.), SAB'04 Swarm Robotics workshop, Springer-Verlag, 2005, pp. 126–142.

[38] H. Wong, V. Kapila, Spacecraft formation flying near Sun-Earth L_2 Lagrange point: Trajectory generation and adaptive output feedback control, in: Proceedings of the American Control Conference, Portland, USA, pp. 2411–2418.